JMEPEG (2012) 21:1943–1948
DOI: 10.1007/s11665-011-0095-x

1059-9495/$19.00

X-Ray Diffraction, Microstructure, and Mössbauer Studies of $Fe_{72}Al_{28}$ Alloy Elaborated by Mechanical Milling

Z. Hamlati, A. Guittoum, S. Bergheul, N. Souami, K. Taibi, and M. Azzaz

(Submitted January 13, 2011; in revised form September 7, 2011)

Nanocrystalline $Fe_{72}Al_{28}$ alloy samples were prepared by mechanical alloying process using planetary high-energy ball mill. The alloy formation and different physical properties were investigated as a function of milling time, *t*, (in the 0-24 h range) by means of X-ray diffraction technique, scanning electron microscopy (SEM), energy dispersive X-ray, and Mössbauer spectroscopy. The complete formation of bcc-FeAl solid solution was observed after 4 h of milling. The lattice parameter quickly increased to a maximum value of 0.291 nm within the first hours of 12 h of milling, then decreased to a value of 0.2885 nm after 24 h. The grain size decreased from 55 to 10 nm, while the strain increased from 0.18 to 0.88%. Grain morphologies at different formation stages were observed by SEM. The Mössbauer spectrum showed the presence of a singlet and sextet after 4 h of milling. The singlet indicated the presence of paramagnetic phase characteristic of A_2 disordered structure and the sextet with a mean hyperfine field, $\langle H_{hf} \rangle$, of 21 T was indicative of ordered DO_3 structure. After 8 h of milling, the paramagnetic phase disappeared allowing the appearance of a sextet. For the higher milling time, i.e., 24 h, the Mössbauer spectrum was analyzed with two components. The first with $\langle H_{hf} \rangle$ equal to 29.9 T and the second with a $\langle H_{hf} \rangle$ value of 10.25 T.

Keywords ball mill, FeAl alloy, Mössbauer effect, nanostructures, ordered and disordered structure, X-ray diffraction

1. Introduction

Mechanical alloying (MA) is a processing technique for synthesis of phases or phase mixtures (Ref 1-3). The MA process leads to an alloy formation by solid-state reactions assisted by severe plastic deformation that occurs during ball milling of the elemental powders. The MA technique helps in overcoming problems such as the large difference in melting points of the alloying components, and unwanted segregation or evaporation that might occur during melting and casting. A great advantage of this process is the fact that it allows the formation of materials far from their thermodynamic equilibrium. In particular, nanocrystalline, quasicrystalline, or amorphous structures can be formed by MA process (Ref 1-3).

Nanocrystalline materials are potentially attractive for many applications because the reduction of grain size to nanometer scale can improve their physical and mechanical properties (Ref 4, 5). Some properties, such as high strength and hardness (Ref 6, 7), ductilization of brittle materials (Ref 8, 9), and enhanced diffusivity (Ref 10) are superior to those of conventional materials. This is possibly due to the nanocrystalline structure. A class of materials widely produced by the MA process is the supersaturated solid solution. Due to the specific chemical composition of this class of materials, their structure orders upon thermal annealing and they transform into intermetallic compound.

Iron-aluminum alloys have drawn the attention of a large number of material scientists for at least the last four decades. Special attention has been given to intermetallic alloys in the composition range of 20-32% Al. For the series of Fe-Al alloys, different soft magnetic and physical properties can be obtained (Ref 11). Apart from the disordered solid solution of Al in α-Fe, two types of superlattices appear in the FeAl alloy systems: the imperfectly ordered B_2 phase and the ordered DO_3 phase. The basic crystal structures of all the phases are the same, i.e., BCC. The alloys in DO_3 structure have interesting magnetic and structural properties, and an extremely good resistance to environmental degradation. For example, Fe-25% Al shows large magnetostriction, while Fe-28% Al shows high magnetic permeability (Ref 11).

Many works have reported the elaboration of nanocrystalline FeAl using different kinds of planetary ball milling systems (Ref 12-20) under different experimental conditions. However, even for the same composition, different phases have been obtained by MA using the same type of mill (Ref 21, 22), because MA is a complex multiparameter process. Thus, despite the same composition of initial powder mixture, various products can be obtained depending on the parameters of the process (type of milling device, ball-to-powder weight ratio, temperature of milling, milling time, milling intensity, etc.) (Ref 3).

The purpose of this article is to study the structural and phase transformations taking place during the MA of $Fe_{72}Al_{28}$ powder mixture in a high-energy ball mill. The effect of milling time on structural, microstructural, and hyperfine properties

Z. Hamlati and **S. Bergheul**, Department of Aeronautics, U.S.D.B., BP270 Blida, Algeria; **A. Guittoum** and **N. Souami**, Nuclear Research Center of Algiers, 2 Bd Frantz Fanon, BP 399 Alger-Gare, Algiers, Algeria; and **K. Taibi** and **M. Azzaz**, Laboratory S.G.M., U.S.T.H.B., Bab-Ezzouar, Algiers, Algeria. Contact e-mail: zinebhamlati@yahoo.fr.

was investigated by X-ray diffraction (XRD), scanning electron microscopy (SEM), and Mössbauer spectroscopy.

2. Experiments

Elemental Fe and Al powders of 99.9% purity and particle sizes smaller than 100 μm were separately weighed and mixed to obtain the desired composition. The MA process was performed in a high-energy planetary ball mill (Retsch PM400). The mixed powder was sealed in a cylindrical vial under an argon atmosphere with stainless steel balls to prevent oxidation phenomena. The ball-to-powder weight ratio was 50:1, while the vial rotation speed was set to 380 rpm. Different milling times ranging from 2 to 24 h were used. To avoid excessive heating during milling, each 15 min of milling was followed by a pause of 15 min under Ar atmosphere. XRD experiments were performed with Philips X-Pert Pro diffractometer in continuous scanning mode using Cu Kα radiation. The X-ray patterns were analyzed using Philips X-Pert Plus software (Ref 23). Each peak was fitted by the pseudo-Voigt (PV) function, a linear combination of Lorentzian (L) and Gaussian (G) functions described by PV $(2\theta) = \gamma L\ (2\theta) + (1 - \gamma)\ G\ (2\theta)$ where γ was a refinable "mixing" parameter called the shape parameter. This parameter described the amount of Gaussian profile versus the amount of Lorentzian profile; and thus described the overall profile shape. The shape parameter of the PV profile function determined the profile. It could vary between 0 (= Gaussian profile) and 1 (= Lorentzian profile). After removing the Cu $K\alpha_2$ radiation from the profiles using the Rachinger method and removing the instrumental broadening using a high purity silicon sample, the physical breadths (β) of the spectral lines were determined for each peak of the pattern.

In order to calculate the mean grain size values from XRD spectra, many methods were used by different researchers. Among those methods, there were Williamson-Hall method, Warren-Averbach method, and Scherrer method, to name few. Each of these methods could be used to estimate the mean value of grain sizes of 10 nm and less (Ref 24).

In the present study, the mean size of the nanocrystallites, $\langle D \rangle$, was calculated according to the Scherrer's formula included in the software and defined by (Ref 25):

$$D = K\lambda/\beta_L \cdot \cos\theta$$

where K represented the shape factor which varied with the crystal shape, λ the wavelength of the Cu $K\alpha_1$ radiation, θ the Bragg angle, and β_L the Lorentzian part of the integral breadth due to the crystallite size.

The mean level of microstrain, $\langle \varepsilon \rangle$, was calculated using the tangent formula included in the software and given by (Ref 26):

$$\langle \varepsilon \rangle = \beta_G/(4\ \tan\theta)$$

where β_G represented the Gaussian part of the integral breadth due to microdistortions, and θ the Bragg angle.

SEM and X-ray microanalysis studies were performed on a Philips XL 30 microscope coupled to an energy dispersive analyzer (EDX). Mössbauer spectra were obtained at room temperature with Wissel instrument in the constant acceleration mode, using a radioactive ^{57}Co source diffused into a Rhodium matrix. Metallic iron was used for energy calibration, and as a reference for isomer shift. Mössbauer spectra were evaluated with the Recoil software using the Voigt-based hyperfine field distribution method (HFD-VB-F) (Ref 27).

3. Results and Discussion

3.1 Structure

The XRD spectrum for the starting powder (labeled 0 h in Fig. 1) shows reflections corresponding to distinct bcc Fe and FCC Al metals. It can be clearly seen that the diffraction peaks are broadened as the milling time increases, indicating a continuous decrease in grain sizes. This broadening was due to the second-order internal stress which acted at the macroscopic level in the crystallites (Ref 28). After 4 h of milling, the reflection peaks corresponding to FCC Al disappeared and the Fe peaks slightly shifted towards lower angles. This proved that Al atoms dissolved in the Fe lattice leading to the formation of Fe (Al) solid solution. The slight angular shift could be attributed to the formation of the new bcc phase, and the first-order internal stress induced by milling. The first-order angular stress acted at the macroscopic level by modifying the lattice parameter, and consequently produced an angular shift of XRD peaks. It is worth noting that for $Fe_{72}Al_{28}$ obtained by MA, the formation of bcc solid solution (Fe-Al) was confirmed by Wolski et al. (Ref 29), Fan et al. (Ref 18), and Oleszak et al. (Ref 30) after 10 h of milling, and by Tang et al. (Ref 19) after 5 h of milling.

The evolution of the lattice parameter for FeAl samples is presented in Fig. 2 as a function of milling time. The figure shows that the lattice parameter monotonously increased within the first hours of milling time, then seemed to reach a stationary value (0.2911 ± 0.0005 nm) when the milling time is extended

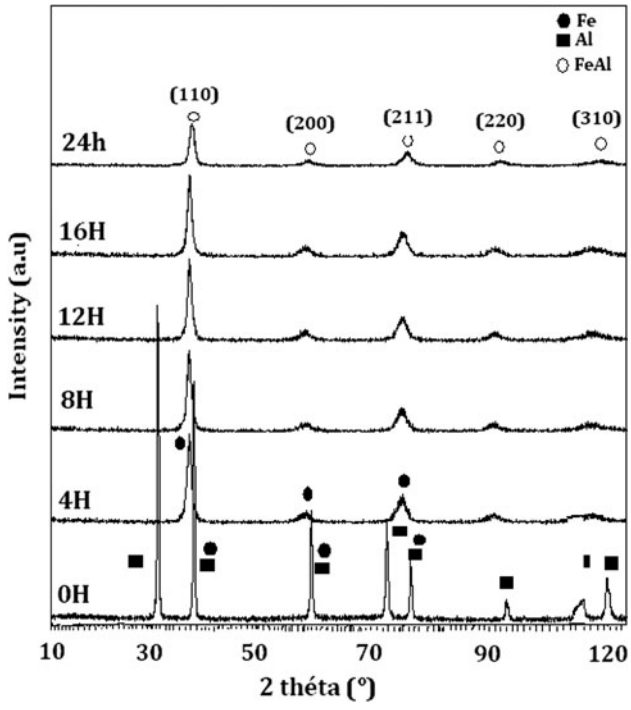

Fig. 1 X-ray diffraction spectra of mechanically alloyed $Fe_{72}Al_{28}$ for various milling times

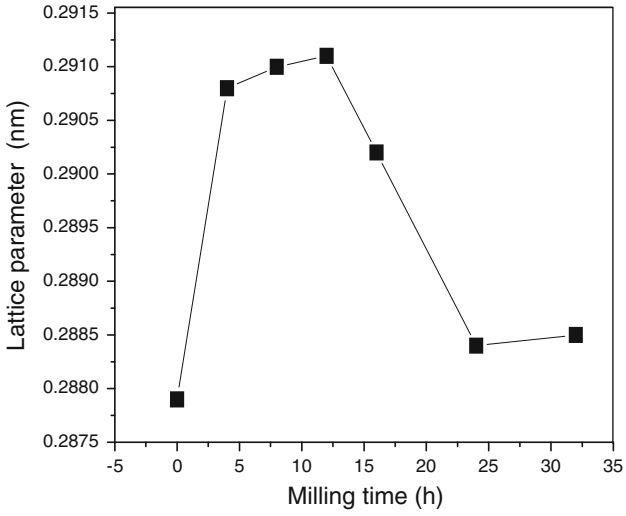

Fig. 2 The lattice parameter, a (nm), as a function of the milling

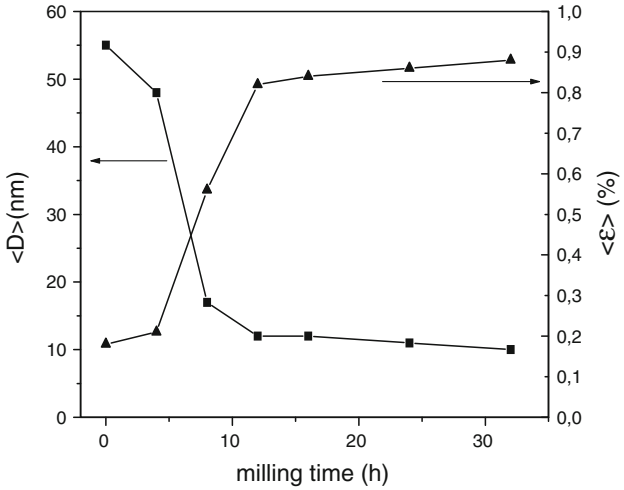

Fig. 3 Mean crystallites size, $\langle D \rangle$ (nm), and mean lattice strain, $\langle \varepsilon \rangle$ (%), as a function of milling time for Fe-28at.%. Al alloy

to 12 h. This behavior might be explained by the diffusion of aluminum atoms into the iron lattice during the first stage of milling (Ref 19, 31). However, the lattice parameter decreased monotonously after 12 h of milling time and reached a constant value of 0.2885 ± 0.0005 nm. This type of decrease in a (nm) was also observed by Fan et al. (Ref 18), and was attributed to the ordered structure (Ref 32).

Figure 3 shows the evolution of the average crystallite sizes $\langle D \rangle$ and the mean level of internal strains $\langle \varepsilon \rangle$ as functions of milling time. It is clear that the crystallite size monotonously decreases as the milling time increases. This decrease in $\langle D \rangle$, accompanied by an increase of the mean internal strain level $\langle \varepsilon \rangle$, is a common behavior of metallic materials obtained through high energy ball milling (Ref 33); it is due to repeated fracturing and cold welding of the powder particles during milling. However, the increase of the mean level strains is due to the shock power which increases with prolonged milling time. Similar dependencies of D and ε parameters on the milling time have been reported by Jartych et al. (Ref 34), and Tang et al. (Ref 19). The $\langle D \rangle$ values of the crystallite size decrease from $\langle D \rangle = 55$ nm for the un-milled powder (0 h, corresponding to the Fe powder) to 10 nm for a milling time of 24 h, while the mean internal strain $\langle \varepsilon \rangle$ values increase from 0.2 to 0.9%.

3.2 Microstructure

Figure 4 shows the morphological evolutions of $Fe_{72}Al_{28}$ alloy as a function of milling time. Figure 4(a), shows the spherical shapes of iron particles of 10 μm size. The presence of irregular structure of 50 μm average size shows the existence of aluminum powder particles (Fig. 4b). After 4 h of milling, new surfaces were formed (Fig. 4c). The initial shape of particles disappeared completely, and their structure became an amalgam of small and large angular-shaped particles with sizes ranging between 10 and 50 μm. After 8 h of milling (Fig. 4d), the formation of lamellar particles is favored (Ref 29); this is certainly related to the fracture and welding phenomena. A further increase in the milling time to 16 h brings the spherical morphology back (Fig. 4e). The increase in the milling time causes the MA progress and refinement of the particles size to continue. For the longest milling time (24 h, see Fig. 4f), the powder particles become equiaxed with small diameters and relatively homogenous in size. This phenomenon is a result of the existence of a balance between the fracture and re-welding processes. EDX analyses were performed on all samples. The standard deviation of the chemical composition of the samples with respect to the nominal ones was less than 1%, and no Cr contamination was found in the samples.

3.3 Mössbauer Spectroscopy

Mössbauer measurements were performed to monitor the process of alloy formation at every stage of milling. Mössbauer spectra at room temperature for different milling times are shown in Fig. 5. The average values of hyperfine magnetic fields $\langle H_{hf} \rangle$ were calculated for all measured samples. For the un-milled sample, the spectrum (not shown here) indicated the presence of a typical sextet with a mean hyperfine field $\langle H_{hf} \rangle$ equal to 32.98 T, which corresponds to the α-Fe present in the starting FeAl powder. By increasing the milling time, the Mössbauer spectra showed different behaviors. Indeed, after 4 h, the Mössbauer spectrum showed the presence of a singlet and sextet. The singlet indicated the presence of a paramagnetic phase, a characteristic of A_2 disordered structure (Ref 35, 36). The sextet, on the other hand, with a mean hyperfine field $\langle H_{hf} \rangle$ of 21 T, was indicative of ordered DO_3 structure (Ref 37, 38).

After 8 h of milling, the paramagnetic phase (singlet line) disappeared completely; and the Mössbauer spectrum was analyzed with one sextet with a mean hyperfine field (H_{hf}) equal to 24.18 T, a characteristic of DO_3' structure (Ref 39). For the sample milled for 16 h; the Mössbauer spectrum exhibited two sextets. The first sextet with $\langle H_{hf} \rangle = 28.5$ T is a characteristic of DO_3 structure. The second sextet with $\langle H_{hf} \rangle$ of 24.8 T is still characterized of DO_3'. For the longer milling time, i.e., 24 h, the Mössbauer spectrum was analyzed with two components. The first one with $\langle H_{hf} \rangle$ equal to 29.9 T was still indicative of ordered DO_3, while the second, with a $\langle H_{hf} \rangle$ value of 10.25 T, was a characteristic of the fine domain B_2 ordered structure (Ref 37, 38).

4. Conclusion

The formation of $Fe_{72}Al_{28}$ alloy from elemental Fe and Al powders was monitored with XRD spectra and Mössbauer

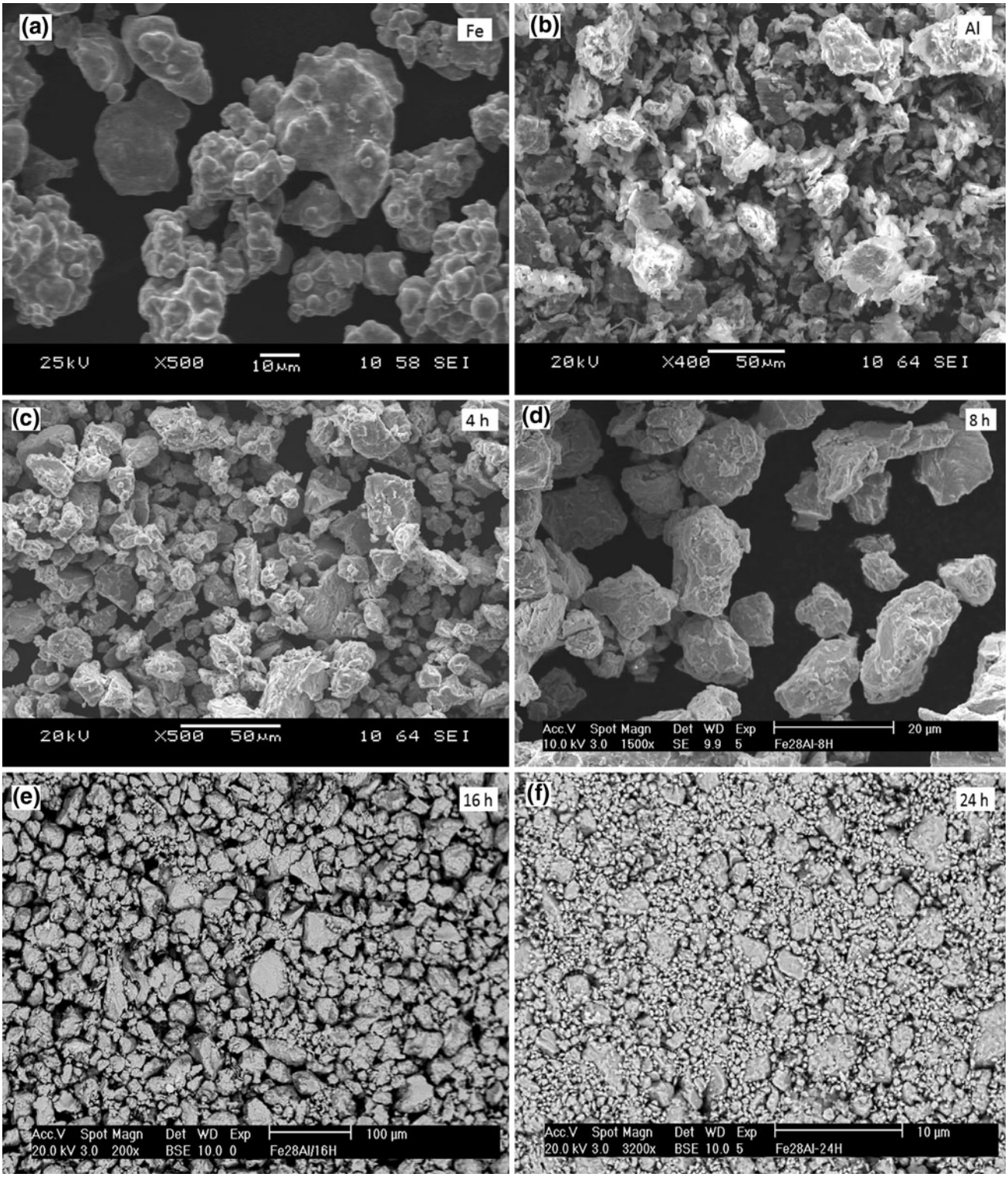

Fig. 4 SEM micrographs of $Fe_{72}Al_{28}$ powders for various milling times: Starting (a) iron and (b) aluminum powders; (c) 4 h; (d) 8 h; (e) 16 h; (f) 24 h

spectroscopy. It was found that, after 4 h of milling, the $Fe_{72}Al_{28}$ was formed. The SEM images taken at different milling times allowed the monitoring of the morphology of the materials at different stages. The Mössbauer spectra showed different behaviors with the increase of milling time. Indeed, after 4 h, the Mössbauer spectrum showed the presence of a sextet, a characteristic of DO_3' structure. For longer milling time, the Mössbauer spectrum was analyzed using two components: The first one having $\langle H_{hf} \rangle$ equal to 29.9 T was indicative of ordered DO_3 and the second one having a $\langle H_{hf} \rangle$ value of 10.25 T was characteristic of the fine B_2 ordered structure domain.

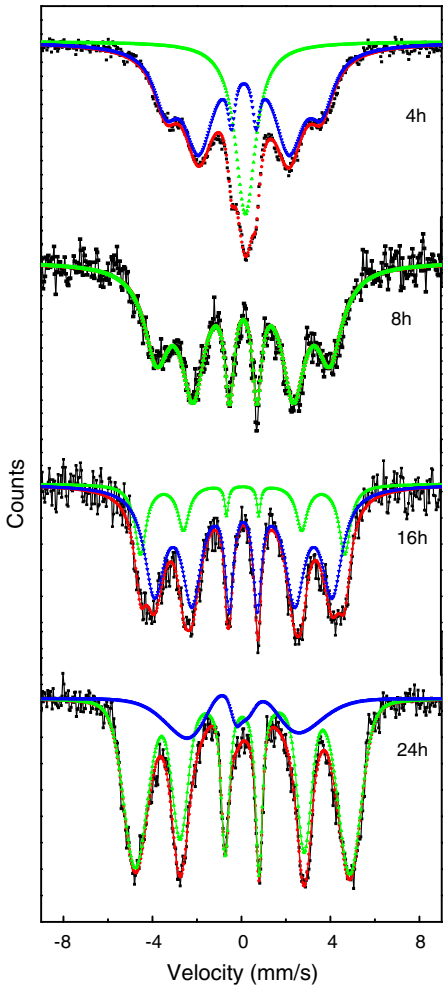

Fig. 5 Room-temperature Mössbauer spectra of $Fe_{72}Al_{28}$ for various milling times

References

1. C.C. Koch, The Synthesis of Non-Equilibrium Structures by Ball-Milling, *Mater. Sci. Forum*, 1992, **88-90**, p 243–262
2. B.S. Murty and S. Ranganathan, Novel Materials Synthesis by Mechanical Alloying Milling, *Int. Mater. Rev.*, 1998, **43**(3), p 101–141
3. C. Suryanarayana, Mechanical Alloying and Milling, *Prog. Mater. Sci.*, 2001, **46**(1–2), p 1–184
4. H. Gleiter, Materials with Ultrafine Microstructures: Retrospective and Perspectives, *NanoStruct. Mater.*, 1992, **1**(1), p 1–19
5. M. Krasnowski and T. Kulik, Nanocrystalline Al-Fe Intermetallics—Light Weight Alloys with High Hardness, *Intermetallics*, 2010, **18**(1), p 47–50
6. G.W. Nieman, J.R. Weertman, and R.W. Siegel, Mechanical Behavior of Nanocrystalline Metals, *NanoStruct. Mater.*, 1992, **1**(2), p 185–190
7. R.W. Siegel and G.E. Fougere, Mechanical Properties of Nanophase Metals, *NanoStruct. Mater.*, 1995, **6**(1–4), p 205–216
8. J. Karch, R. Birringer, and H. Gleiter, Ceramics Ductile at Low Temperature, *Nature*, 1987, **330**, p 556–558
9. S.X. McFadden, R.S. Mishra, R.Z. Valiev, A.P. Zhilyaev, and A.K. Mukherjee, Low-Temperature Superplasticity in Nanostructured Nickel and Metal Alloys, *Nature*, 1999, **398**, p 684–686
10. R. Birringer, Nanocrystalline Materials, *Mater. Sci. Eng. A*, 1989, **117**, p 33–43
11. J.C. wang, D.G. Liu, M.X. Chen, and X.X. Cai, The Positron Study of the Process of Heat-Treatments of Three Important Fe-Al Alloys, *Scripta Metall.*, 1991, **25**(11), p 2581–2583
12. D. Oleszak and P.H. Shingu, Amorphous Fe-Al Alloys Obtained by mechanical Alloying, *Mater. Sci. Forum*, 1997, **235–238**, p 91–96
13. B. Huang, K.N. Ishihara, and P.H. Shingu, Metastable Phases of Al-Fe System by Mechanical Alloying, *Mater. Sci. Eng. A*, 1997, **231**(1–2), p 72–79
14. Y. Zou, S. Saji, and T. Kusabiraki, Fast Amorphization and Crystallization in Al-Fe Binary System by High-Energy Ball Milling, *Mater. Res. Bull.*, 2002, **37**(1), p 123–131
15. Q. Zeng and I. Baker, Magnetic Properties and Thermal Ordering of Mechanically Alloyed Fe-40 at% Al, *Intermetallics*, 2006, **14**(4), p 396–405
16. M. Mhadhbi, M. Khitouni, L. Escoda, and J.J. Suñol, X-ray Studies of Structure Defects in Nanostructured FeAl Alloy, *Mater. Lett.*, 2010, **64**(16), p 1802–1805
17. M. Mhadhbi, M. Khitouni, L. Escoda, J.J. Suñol, and M. Dammak, Microstructure Evolution and Mechanical Properties of Nanocrystalline FeAl Obtained by Mechanical Alloying and Cold Consolidation, *J. Alloys Compd.*, 2011, **509**(7), p 3293–3298
18. R. Fan, J. Sun, H. Gong, K. Sun, and W. Wang, Structural Evolution of Mechanically Alloyed Nanocrystalline Fe-28Al Powders, *Powder Technol.*, 2005, **149**(2-3), p 121–126
19. W.M. Tang, Z.X. Zheng, H.J. Tang, R. Ren, and Y.C. Wu, Structural Evolution and Grain Growth Kinetics of the Fe-28Al Elemental Powder During Mechanical Alloying and Annealing, *Intermetallics*, 2007, **15**(8), p 1020–1026
20. E. Jartych, Local Atomic Order in Nanocrystalline Fe-Based Alloys Obtained by Mechanical Alloying, *J. Magn. Magn. Mater.*, 2003, **265**(2), p 176–188
21. S. Enzo, G. Mulas, and R. Frattini, The Structure of Mechanically Alloyed $Al_xFe_{(1-x)}$ End-Products After Annealing, *Mater. Sci. Forum*, 1998, **269-272**, p 385–390
22. F. Cardellini, V. Contini, R. Gupta, G. Mazzone, A. Montone, A. Perin, and G. Principi, Microstructural Evolution of Al-Fe Powder Mixtures During High-Energy Ball Milling, *J. Mater. Sci.*, 1998, **33**(10), p 2519–2527
23. X-Pert Plus software, *Program for Crystallography and Rietveld Analysis*, Philips Analytical, Almelo, 1999
24. I. Lucks, P. Lamparter, and E.J. Mittemeijer, An Evaluation of Methods of Diffraction-Line Broadening Analysis Applied to Ball-Milled Molybdenum, *J. Appl. Crystallogr.*, 2004, **37**, p 300–311
25. A. Patterson, The Scherrer Formula for X-Ray Particle Size Determination, *Phys. Rev.*, 1939, **56**(10), p 978–982
26. A.R. Stokes and A.C.J. Wilson, Diffraction of X-rays by Distorted Crystal Aggregates. I, *Proc. Phys. Soc. Lond.*, 1944, **56**, p 174
27. K. Lagarek and D. Rancourt, *Recoil Software*, Physics Department, University of Ottawa, Ottawa, 1998
28. L. Castex, J.L. Lebrun, G. Maeder, and J.M. Sprauel, Mesures de contraintes résiduelles par diffraction X, Publications scientifiques et techniques, 22, ENSAM, Paris, 1981, p 51 (in French)
29. K. Wolski, G. Caer, P. Delcroix, R. Fillet, F. Thévenot, and J. Le Coze, Influence of Milling Conditions on the FeAl Intermetallic Formation by Mechanical Alloying, *Mater. Sci. Eng.*, 1996, **207**(1), p 97–104
30. D. Oleszak and H. Matyja, Nanocrystalline Fe-based Alloys Obtained by Mechanical Alloying, *NanoStruct. Mater.*, 1995, **6**(1–4), p 425–428
31. E. Jartych, J.K. Zurawicz, D. Oleszak, M. Pekata, J. Sarzynski, and M. Budzynski, Magnetic Properties and Structure of Nanocrystalline $Fe_{70}Al_{30}$ Alloy Prepared by Mechanosynthesis, *J. Magn. Magn. Mater.*, 1998, **186**(3), p 299–305
32. R.W. Cahn, Lattice Parameter Changes on Disordering Intermetallics, *Intermetallics*, 1999, **7**(10), p 1089–1094
33. R. Koohkan, S. Sharafi, H. Shokrollahi, and K. Janghorban, Preparation of Nanocrystalline Fe-Ni Powders by Mechanical Alloying Used in Soft Magnetic Composites, *J. Magn. Magn. Mater.*, 2008, **320**(6), p 1089–1094
34. E. Jartych, J.K. Zurawicz, D. Oleszak, and M. Pekala, Magnetic Properties and Structure of Nanocrystalline Fe-Al and Fe-Ni Alloys, *NanoStruct. Mater.*, 1999, **12**(5-8), p 927–930
35. D.S. Schmool, E. Araujo, M.M. Amado, M. Alegria Feio, D. Martin Rodriguez, J.S. Garitaonandia, and F. Plazaola, Magnetic Properties of the Fe-rich Fe_xAl_{1-x} Alloy System, *J. Magn. Magn. Mater.*, 2004, **272–276**, p 1342–1344
36. V. Sebastian, N. Lakshmi, and K. Venugopalan, Structural and Magnetic Properties of Mechanically Alloyed Fe-66 at%Al, *Intermetallics*, 2007, **15**(8), p 1006–1012
37. H.C. Verma and S. Suwas, Mossbauer Studies of Phase Stability in Mechanically Stressed Fe-28 at% Al Alloy, *J. Magn. Magn. Mater.*, 2000, **212**(3), p 361–367

38. S. Sarkar and C. Bansal, Atomic Disorder-Order Phase Transformation in Nanocrystalline Fe-Al, *J. Alloys Compd.*, 2002, **334**(1–2), p 135–142

39. M. Krasnowski, A. Grabias, and T. Kulik, Phase Transformations During Mechanical Alloying of Fe-50% Al and Subsequent Heating of The Milling Product, *J. Alloys Compd.*, 2006, **424**(1–2), p 119–127